Carrera Unified Formulation for Free-Vibration Analysis of Aircraft Structures

CUF Based Variable Kinematic Models for Free Vibration Analysis of Aircraft Structures [1]

Carrera Erasmo[2]
Politecnico di Torino, Corso Duca degli Abruzzi, 24, 10129, Torino, Italy.

Zappino Enrico[3]
Politecnico di Torino, Corso Duca degli Abruzzi, 24, 10129 Torino, Italy.

Advanced structural models, based on variable one-(1D), two-(2D) and three-dimensional (3D) kinematics, are proposed in this paper and applied to the analysis of the free vibration of reinforced aircraft shell structures. The used models go beyond classical structural theories that is, Euler-Bernoulli (for 1D beams) and Kirchhoff (for 2D plates) type assumptions. The order of the expansion of the displacement fields over the cross section (1D case) and along the plate thickness (2D case) is in fact a free parameter of the problem. In this paper, Lagrange polynomials are used to build such expansions and, as a consequence, only displacements are used as the problem unknowns (no rotations or derivatives of displacements, which are typical of 1D-2D classical theories are introduced). The finite element method (FEM) is used to provide numerical solutions. The related arrays and the governing dynamical equations are written in terms of a few fundamental nuclei according to the Carrera Unified Formulation, CUF. Classical 3D FE solid models are also considered. 1D, 2D and 3D finite elements are easily connected to each other to make the most appropriate computational model of the reinforced shell structures. The capability to use the same fundamental nucleus to derive FE matrices of 1D, 2D and 3D elements of the present

---

[1] The contents of this paper were partially presented at the 54rd AIAA/ASME/ASCE/AHS/ASC Structures, Structural Dynamics, and Materials Conference (SDM), Boston, Massachusetts, USA, April 8-11, 2013

[2] Professor, Mechanical and Aerospace Engineering Department, Corso Duca degli Abruzzi, 24, 10129 Torino, Italy, erasmo.carrera@polito.it.

[3] Research Assistant, Mechanical and Aerospace Engineering Department, Politecnico di Torino, Corso Duca degli Abruzzi, 24, 10129 Torino, Italy, enrico.zappino@polito.it.

model is unique as it is usually not available in other FE formulation, that is, no *ad hoc* techniques are required in the present case to couple finite elements with different kinematics. Three main benchmarks have been analyzed: a plate stiffened by means of bidirectional I-stiffeners, a simplified model of a complete aircraft and a fuselage-wing connection. Comparison with commercial FE software (MSC Nastran) is provided for most of the quoted numerical investigations. The modal assurance criterion has been used to compare the free vibration modes of the different models. The present mathematical models appear closer to reality and cheaper, from the computational point of view, than those of other existing formulations. CUF based FEs do not require the definition of virtual lines (beam axes) or virtual surfaces (plate reference surfaces), and only physical lines/surfaces are therefore used.

Nomenclature

$\mathbf{\Lambda}$	Global rotation matrix
$\mathbf{\Lambda_x}$	Rotation matrix with respect to x
$\mathbf{\Lambda_y}$	Rotation matrix with respect to y
$\mathbf{\Lambda_z}$	Rotation matrix with respect to z
$\boldsymbol{b}$	Differential operator, [-]
$\boldsymbol{C}$	Material coefficients matrix, $[Pa]$
$\boldsymbol{K}^{ij\tau s}$	Stiffness matrix fundamental nucleus
$\boldsymbol{M}^{ij\tau s}$	Mass matrix fundamental nucleus
$\boldsymbol{u}$	Displacement vector, [m]
δ	Virtual variation
$\delta \mathbf{u}_{js}$	Virtual variation of the nodal displacements
ν	Poisson's Ratio, [-]

ϕ Rotation angle with respect to y, [deg]

ρ Material density, $[Kg/m^3]$

σ Stresses vector, [Pa]

$\mathbf{u}_{i\tau}$ Nodal displacements

θ Rotation angle with respect to x, [deg]

ε Strains vector, [-]

ξ Rotation angle with respect to z, [deg]

E Young's modulus, [Pa]

F_τ, F_s Structural model approximation functions

L_{ine} Inertial work, [J]

L_{int} Internal work, [J]

N_i, N_j FEM shape functions

u_x, u_y, u_z Displacement components, [m]

I. Introduction

The analysis of complex primary, secondary and complete aircraft structures requires the use of adequate numerical models. These mainly consist of thin-walled components reinforced with stringers and ribs. Assumptions on stress/strain/displacement fields are often introduced to simplify the analysis of panels, ribs and longerons. One very well known method is the one introduced by Argyris and Kelsey [1], which consists of a "Force method". This approach separates the roles of the panels, where only constant shear stresses are assumed to be present, and the reinforcements, where only linear distributions of normal stresses are allowed along their length. The "Force method" has been described in details in many textbooks, the one by Bruhn [2] is still used in the preliminary design of aeronautical structures, as shown by Carrera [3].

The development of computers and computational mechanics has lead to the automatic calculation of any complex structure. The most reliable and robust computational approach currently employed in the analysis of aircraft structures is, without doubt, the Finite Element Method (FEM).

Dozens of books are available on this method and the one by Zienkiewics deserves mentioning [4]. Each structural component is discretized into a finite number of elements, and each of these can be analyzed using one- (beams/rods)- , two- (plates/shells) or three-(solids) dimensional elements. The formulation of each element (stiffness matrix, mass matrix, load vector etc.) is obtained from classical structural theories, such as those proposed by Euler-Bernoulli [5] (or Timoshenko [6]) in the case of beams, or the Kirchhoff-Love [7] (or Reissner-Mindlin [8, 9]) theories in the case of plates/shells. Three-dimensional elements do not require structural models, but they can be used to directly solve the equation of elasticity in their complete formulation, as shown by Argyris [10].

The formulation of classical FEM models, which are implemented in most FE commercial software, assumes that the deformation at each point can be described using only three displacements and three rotations. However, this is not true for solids; in this cases, only three-displacements are usually used as degrees of freedom, DOF. Nevertheless, in classical models, the FE nodes lie on reference axes/surfaces that consist of virtual/mathematical entities. For this reason, the connection/junction of 1D/2D/3D elements requires the use of some mathematical 'tricks', such as the use of offsets, so as to be representative of the real structures. In the framework of classical FEM, the connection of 1D to 2D FEs and 1D/2D to 3D FEs can be obtained when the matrices are assembled, that is, when the stiffness corresponding to the shared nodes are added together. Other approaches can be used to join different structural models. One example is the use of Lagrange multipliers, as in [11], which allows the displacement compatibility to be imposed at one or more points. A more effective approach is that known as the *Arlequin* method, which was proposed by Ben Dhia [12, 13]. This method introduces an overlapping zone between two models, and the equivalence is imposed on this domain. McCune *et al.* [14] introduced a mixed-dimensional coupling scheme, based on geometrical assumptions, while Garusi and Tralli [15] used a transition element to derive solid-to-beam and plate-to-beam connections. Song and Hodges [16] used an asymptotic approach to join beam and solid elements. A variational approach able to join incompatible kinematics was introduced by Blanco *et al.* [17] while. Davila [18] proposed a penalty method to join solid and shell elements, while Shim *et al* [19] used multi-point constraint equations to force the congruence at the interface of elements with different kinematics.

Some approximate methods consider the reinforcements smeared over the plate; these approaches are presented in the works by Luan *et al.*[20] and Edalat *et al.*[21] but, in this case, the results do not provide detailed information about the behaviour of each component of the structure. More detailed models have been presented by Mustafa and Ali [22] and Edward and Samer [23], who introduced some *ad hoc* finite element models that are able to deal with reinforced structures. A dynamic analysis is crucial in aircraft design. The dynamic response, can in fact have a great effect on the performances of an aircraft. Aeroelasticity, flight dynamics and flight comfort are only a few aspects in which structural dynamics may play an important role.

The use of advanced structural models allows the accuracy of the analysis to be improved when complex physical phenomena have to be included. An impulse to the development of advanced theories for structures took place with the developments of multi-layered structure theories such as laminated composites, which exhibit a rather complex strain/stress/displacement field (mostly along the layer thickness direction). Refined structural models can be developed using different approaches. The asymptotic approach was used by Yu *et. al.* [24, 25] to derive advanced structural models, this approach allows the kinematic model to be derived via an asymptotic analysis. In contrast, the axiomatic theories assume the kinematic model *a priori*. Among the axiomatic theories, the Carrera Unified Formulation (CUF), which was proposed by the first author in [26], [27, 28], [29], [30] and which has recently been published in three books [31–33] is considered in this paper. As one of its main features, CUF permits the equations of any refined 1D, 2D or 3D theory to be expressed in terms of a few fundamental nuclei, FNs, whose forms do not formally depend on the assumptions (type of functions or order) that have been used to describe the displacement field over the cross-section (in one-dimensional models) and through the thickness (in one-dimensional models). Since the order of the theories is a free parameter of the problem, and the form of the FNs is the same for the 1D, 2D and 3D cases, CUF has often been referred to as a 'variable kinematic' tool to analyze structures.

The performance of the refined models obtained through the CUF have been shown in many works [34–36]. In the work by Carrera *et al.*[37], the Lagrange multiplier method was used to connect 1D finite elements with different kinematics. Some results on the Arlequin method applied

to CUF have been shown by Biscani *et al.*[38], where a mixed two/three-dimensional model has been derived. Both methods require the introduction of new unknowns into the problem, which makes the stiffness matrix not positive semi-definite. For this reason, some numerical issues can arise when these approaches are used. The present paper introduces a new approach that is able to connect refined structural models with variable kinematics. Unlike the existing approaches, the use of Lagrange functions make it possible to obtain only displacements as the degrees of freedom, that is, no *ad hoc* formulations are required to connect different models. The compatibility of the displacements is imposed during the matrix assembly procedure, when the stiffness of the shared nodes are added together in the classical way. The words *variable kinematics* in this manuscript are extended to include CUF FE elements with both different displacement fields and dimensions (1D, 2D or 3D). Models with only displacements as the unknowns are herein considered. The theoretical models are described and the coupling strategy is introduced in the first part of the manuscript. The variable kinematics models are then assessed and used to analyze a plate stiffened by means of bidirectional I-stiffeners, a simplified complete aircraft model and a fuselage-wing connection. The results are compared with those from classical finite element formulations and the Modal Assurance Criterion, MAC, is used to compare the modal shapes.

II. Refined Finite Element Formulation

The one-, two- and three-dimensional elements used in the present paper are derived in the framework of the Carrera Unified Formulation. In this section the theoretical approach is introduced, a more comprehensive description of these models can be found in [33].

A. Preliminaries

The fundamental equations and the nomenclature used in the following pages are introduced in this section. The displacement vector is denoted as follows:

$$\mathbf{u}^T = (u_x,\, u_y,\, u_z) \tag{1}$$

where u_x, u_y and u_z are the components of the displacement vector in the three directions. The strains and stresses vectors are defined as:

$$\varepsilon^T = (\varepsilon_{xx}, \varepsilon_{yy}, \varepsilon_{zz}, \varepsilon_{xy}, \varepsilon_{xz}, \varepsilon_{yz}), \tag{2}$$

$$\sigma^T = (\sigma_{xx}, \sigma_{yy}, \sigma_{zz}, \sigma_{xy}, \sigma_{xz}, \sigma_{yz}). \tag{3}$$

The relation between strains and displacements can be written using the geometrical equation:

$$\boldsymbol{\varepsilon = bu}, \tag{4}$$

where $\boldsymbol{b}$ is a differential operator, the explicit form of $\boldsymbol{b}$ can be found in [33]. The Hooke's law permits to derive the relation between stresses and strains:

$$\boldsymbol{\sigma = C\varepsilon}, \tag{5}$$

where $\boldsymbol{C}$ is the stiffness coefficients matrix of the material.

B. Kinematic assumptions

The structural models used in the present paper are derived introducing an approximation on the displacement field. An axiomatic approach is used in the present work, that is, the formulation of the displacement field is assumed *a priori*. The generic three-dimensional displacement field can be written as follows:

$$\mathbf{u} = \mathbf{u}(x, y, z). \tag{6}$$

where $\mathbf{u}(x, y, z)$ is a three-dimensional function solution of the problem. When the structure has a dimension, z, which can be neglected with respect to the others, x and y, it is possible to introduce a plate/shell model, in this case the Equation (6) can be reduced to:

$$\mathbf{u} = \mathbf{u}_\tau(x, y) F_\tau^{1D}(z), \qquad \tau = 1 \dots M, \tag{7}$$

where F_τ^{1D} represents a generic function expansion used to approximate the displacement field through the thickness, and M is the number of terms in the expansion. If two dimensions, x and z, are negligible with respect to the other, y, it is possible to reduce Equation (6) in the form:

$$\mathbf{u} = \mathbf{u}_\tau(y) F_\tau^{2D}(x, z), \qquad \tau = 1 \dots M \tag{8}$$

where F_τ^{2D} represents the function expansion used to approximate the solution over the cross-section of the beam model, and M is the number of terms in the expansion. Whatever is the problem considered, one-, two- or three-dimensional, the functions F_τ can be assumed *a priori*. The choice of F_τ depends on the structural model to be used in the analysis. The function u_τ is the unknown of the structural problem, in the present paper the solution is obtained using the FE method therefore the domain is discretizated in a finite number of elements where the solution is approximated using the shape functions, N_i. The generic displacement field can be written as:

$$\mathbf{u} = \mathbf{u}_{i\tau} N_i F_\tau, \qquad \tau = 1 \dots M; \qquad i = 1 \dots N_n. \tag{9}$$

Where the index i comes from the FE model and the index τ comes from the kinematics used in the structural model approximation. N_n is the number of nodes in the finite element. $\mathbf{u}_{i\tau}$ is the coefficient of the expansion and it is also the unknown of the problem. The indicial form showed in Equation (9) is common for all the structural models, the choice of N_i and F_τ makes the difference:

$$3D \longrightarrow \mathbf{u} = \mathbf{u}_i N_i(x, y, z) \tag{10}$$

$$2D \longrightarrow \mathbf{u} = \mathbf{u}_{i\tau} N_i(x, y) F_\tau^{1D}(z) \tag{11}$$

$$1D \longrightarrow \mathbf{u} = \mathbf{u}_{i\tau} N_i(y) F_\tau^{2D}(x, z) \tag{12}$$

Once introduced the approximation due to the structural model, the classical FE approach is used to solve the problem. The virtual variation of the displacements can be written in a similar form

using the indexes j and s,

$$\delta\mathbf{u} = \delta\mathbf{u}_{js} N_j F_s, \qquad s = 1 \dots M; \qquad j = 1 \dots N_n; \tag{13}$$

where δ denotes the virtual variation. The shape functions used in the one-, two- and three-dimensional models are quadratic Lagrange functions. The equations of the N_i can be found in [39]. The choice of F_τ depends on the structural model used. In the following sections are reported the kinematic assumptions used in the present paper for the one- and two-dimensional model while the three-dimensional model does not require any approximation other than the FEM.

1. One-dimensional model

One-dimensional models require to introduce an approximation over the cross-section. If the reference axis of the beam is assumed to be the $y - axis$, where FEM is used to obtain the solution, an expansion can be used to approximate the solution over the cross-section on the plane $x - z$, as shown in Figure 1.

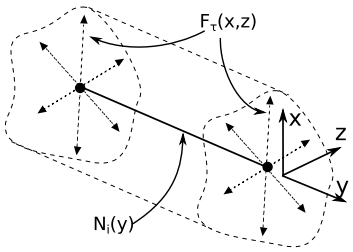

Fig. 1 Representation of the one-dimensional approximation. Function F_τ^{2D} is used over the cross-section while N_i along the axis.

Different expansions can be used over the cross-section, the present model uses the quadratic two-dimensional Lagrange functions to describe the solution over the cross-section, this approach was presented in [40, 41]. The displacement field can be written as:

$$\mathbf{u} = \mathbf{u}_{i\tau} N_i(y) F_\tau^{2D}(x, z). \tag{14}$$

Where $F_\tau^{2D}(x, z)$ is the generic 2D Lagrange function. The use of Lagrange functions permit to have only displacements as unknowns.

2. Two-dimensional model

Two-dimensional models use the FEM to solve the problem over the reference surface, in this case the plane $x-y$, and introduce a function expansion to approximate the displacements through the thickness, see Figure 2.

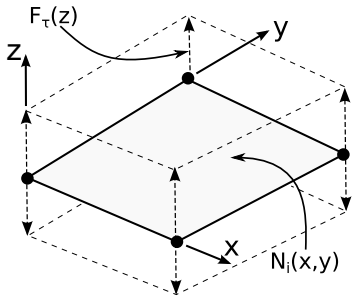

Fig. 2 Representation of the two-dimensional approximation. Function F_τ^{1D} is used through the thickness while N_i over the reference surface.

One-dimensional Lagrange functions are used to approximate the solution through the $axis-z$. The details of this model can be found in [26, 32]. The displacement field can be written as:

$$\mathbf{u} = \mathbf{u}_{i\tau} N_i(x,y) F_\tau^{1D}(z). \tag{15}$$

Where $F_\tau^{1D}(z)$ is the generic term of the expansion over the thickness. The use of Lagrange functions makes that in each node considered over the thickness the unknowns are only displacements.

C. Governing Equations via Unified Formulation

The Principle of Virtual Displacement, PVD, can be used to derive the governing equations of the dynamic problem:

$$\delta L_{int} + \delta L_{ine} = 0 \tag{16}$$

Where L_{int} denotes the internal work while L_{ine} stands for the inertial work. δ is the virtual variation. Because only free vibrations are investigated in the present paper, the external work is not considered. The explicit form of the internal work is obtained using the equations introduced

in the previous sections:

$$\delta L_{int} = \int_V \delta\varepsilon^T \sigma \; dV \tag{17}$$

If the generic displacement field reported in Equations 9 is considered the internal work becomes:

$$\delta L_{int} = \delta q_{js}^T \underbrace{\left(\int_V F_s N_j \boldsymbol{b}^T \boldsymbol{C} \boldsymbol{b} N_i F_\tau dV \right)}_{\boldsymbol{K}^{ij\tau s}} q_{i\tau} = \delta q_{js}^T \boldsymbol{K}^{ij\tau s} q_{i\tau} \tag{18}$$

The indices j and s are used for the virtual variation of the displacements. The inertial work can be obtained using the same approach:

$$\delta L_{ine} = \int_V \delta \boldsymbol{u}^T \rho \ddot{\boldsymbol{u}} dV \tag{19}$$

where $\ddot{u}$ is the acceleration. When the displacement field reported in Equation 9 is considered, Equation 19 becomes:

$$\delta L_{ine} = \delta q_{js}^T \underbrace{\left(\int_V F_s N_j \rho N_i F_\tau dV \right)}_{\boldsymbol{M}^{ij\tau s}} \ddot{q}_{i\tau} = \delta q_{js}^T \boldsymbol{M}^{ij\tau s} \ddot{q}_{i\tau} \tag{20}$$

Equations 18 and 20 are valid whatever model is considered. No assumptions are made on the functions F and N therefore these equations deal with one-, two- as well as three-dimensional models.

$\boldsymbol{K}^{ij\tau s}$ and $\boldsymbol{M}^{ij\tau s}$ are the fundamental nuclei of the stiffness and mass matrices. These are 3×3 matrices and they have a fixed form. The global matrices can be obtained considering all the combination of the indices i, j, τ and s. More details about the fundamental nucleus formulation and their explicit forms can be found in [33].

D. Rotation of fundamental nucleus

The analysis of complex structures requires to rotate the finite elements in any direction and to compute the stiffness in a given reference system, that is, the displacements have to be expressed

in the same, global, reference system. The matrices can be written in the global reference system using a rotation matrix with respect to the local reference system. The rotation matrices are:

$$\boldsymbol{\Lambda_x} = \begin{bmatrix} 1 & 0 & 0 \\ 0 & cos(\theta) & sin(\theta) \\ 0 & -sin(\theta) & cos(\theta) \end{bmatrix}, \quad \boldsymbol{\Lambda_y} = \begin{bmatrix} cos(\phi) & 0 & sin(\phi) \\ 0 & 1 & 0 \\ -sin(\phi) & 0 & cos(\phi) \end{bmatrix}, \quad \boldsymbol{\Lambda_z} = \begin{bmatrix} cos(\xi) & -sin(\xi) & 0 \\ sin(\xi) & cos(\xi) & 0 \\ 0 & 0 & 1 \end{bmatrix} \tag{21}$$

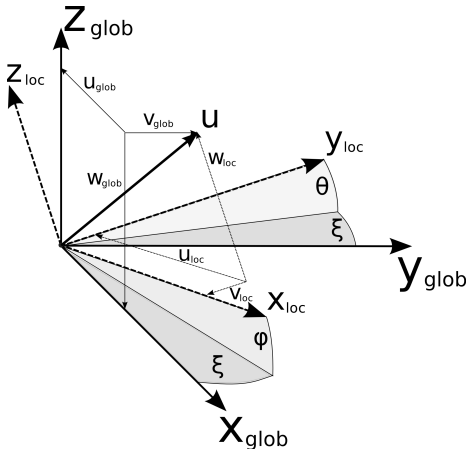

Fig. 3 Representation of the angles of rotations.

where θ, ϕ and ξ are the rotation angles around the axis x,y,and z, as shown in Fig. 3 The displacement vector in the global reference system, $\boldsymbol{u}_{glob}$, can be written as:

$$\boldsymbol{u}_{glob} = \boldsymbol{\Lambda_x}\boldsymbol{\Lambda_y}\boldsymbol{\Lambda_z}\boldsymbol{u}_{loc} = \boldsymbol{\Lambda}\boldsymbol{u}_{loc} \tag{22}$$

Therefore, the fundamental nucleus in the global reference system becomes:

$$\boldsymbol{K}^{ij\tau s}_{glob} = \boldsymbol{\Lambda}^T \boldsymbol{K}^{ij\tau s}_{loc} \boldsymbol{\Lambda} \tag{23}$$

III. Variable kinematic modes assembly

The refined models introduced in the present paper share a common feature, that is, they all have only displacements as the degrees of freedom. This property allows models with different dimensions to be combined by imposing the equivalence of the displacements at one or more nodes, as in the classical FE approach, more details can be found in the book by Oñate [39].

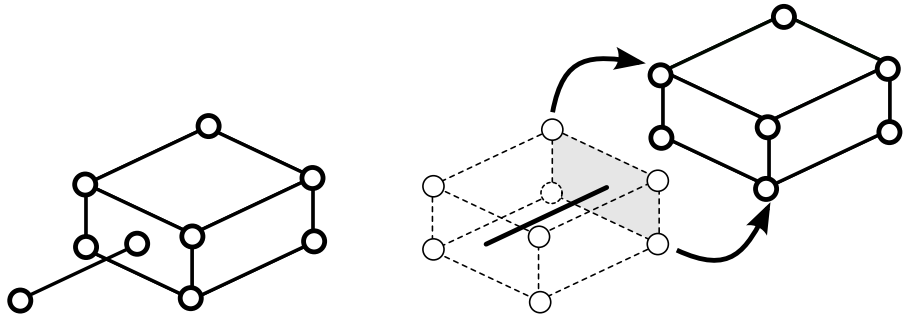

(a) Classical approach (b) Present approach

Fig. 4 1D/3D variable kinematic model assembling.

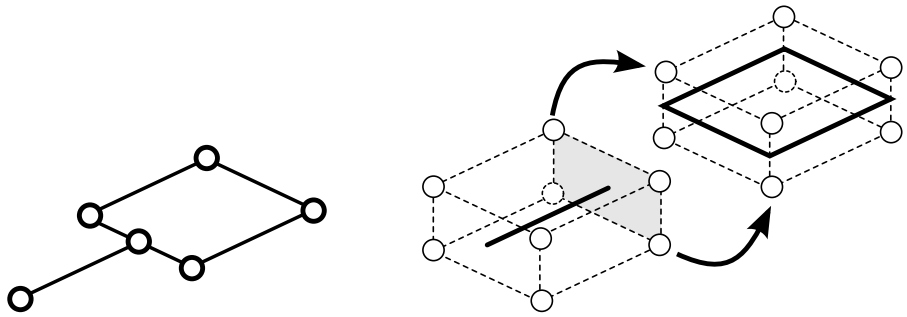

(a) Classical approach (b) Present approach

Fig. 5 1D/2D variable kinematic model assembling.

Figure 4 shows the assembly of 1D and 3D elements. Figure 4a shows the classical approach, which is the procedure that is commonly used in FE software. In this case, the beam nodes do not correspond to any nodes of the solid element, and some rigid connections between the beam and the solid nodes are usually introduced in order to ensure congruency of the displacements at these points. Figure 4b shows the present approach. In this case, the beam has four nodes over the cross-section and, as a result, the 1D and 3D nodes can be assembled easily. A similar situation can be seen in Figure 5. In this case, a beam element has to be assembled with a plate element. In the classic approach, Figure 5a, the assembly would not be possible unless *ad hoc* techniques were introduced. If the present approach is used, Figure 5b, the four nodes on the beam cross-section can easily be assembled with those of the plate element, which has 2 nodes through the thickness. Finally, a variable kinematic model, including a two-dimensional and a solid element, is presented in Figure 6. As in the previous cases, the plate element can easily be connected to the solid when only displacement variables are used in both the 2D and 3D formulations. If a classical approach is considered, 6a, the assembly of the two elements requires the introduction of additional rigid elements or a mesh refinement.

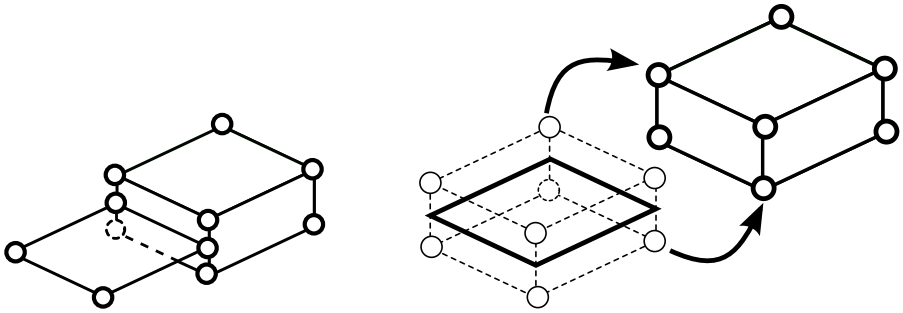

(a) Classical approach (b) Present approach

Fig. 6 2D/3D variable kinematic model assembling.

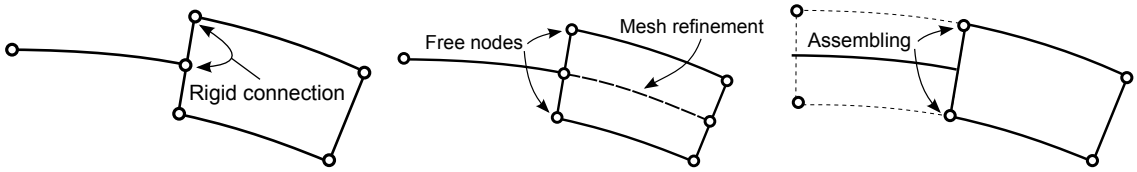

(a) Rigid connection (b) Mesh refinement (c) Present approach

Fig. 7 Interface between a beam and a solid model, coupling approaches.

The use of the present approach allows the interface between different models to be represented properly. Figure 7 shows three different approaches to the modelling of a beam under a bending load. In all the cases, a beam element is connected to a solid element. In Figure 7a, a classical beam element is connected to a solid element via rigid connections; this approach is time consuming in the pre-processing phase, and displacements at the interface are assumed to be dominated by the beam element; the cross section is therefore still rigid. Figure 7b shows how with a refined mesh, it is possible to directly connect the beam element to a solid element but the two external nodes are completely free to move at the interface, ad, as a result, the congruence of the displacements at the interface is not ensured. Finally, Figure 7c shows the present approach. It is clear that the present refined beam model guarantees the displacement congruence. In addiction, the refined beam element takes into account cross-section deformation.

IV. Numerical analysis

In this section, different structures are investigated to demonstrate the accuracy of the present models. A simple cantilevered beam is used to assess the variable kinematic model. More complex structures are therefore considered and a complex aircraft structure is investigated. Only metallic

materials are considered. The results are reported in terms of frequency and modal shapes and are compared with those from classical 2D and 3D FEM models. Where possible, the modal shapes are compared using the Modal Assurance Criterion, which is also called MAC. MAC has the following form:

$$MAC = \frac{[\boldsymbol{\zeta}_p(i)^T \boldsymbol{\zeta}_r(j)]^2}{[\boldsymbol{\zeta}_p(i)^T \boldsymbol{\zeta}_p(i)][\boldsymbol{\zeta}_r(j)^T \boldsymbol{\zeta}_r(j)]} \tag{24}$$

where $\boldsymbol{\zeta}_p(i)$ is the $i-th$ eigenvector from the present model and $\boldsymbol{\zeta}_r(j)$ is the $j-th$ eigenvector from the reference model. The MAC value is between 0 and 1. A MAC number equal to 1 means that the two modes match perfectly.

A. Variable kinematic model assessment

A cantilever beam has been considered to asses the present variable kinematic model. The physical model is reported in Fig.8. The dimensions of the beam are: length $h = 3\ m$, width $b = 0.2\ m$ and height $a = 0.1\ m$. The structure has not constraints. The material considered in the analysis has an elastic modulus $E = 71.7\ GPa$, a Poisson ratio $\nu = 0.3$ and a density $\rho = 2700\ Kg/m^3$.

Different variable kinematic models are presented. Fig.8 shows that all the three structural

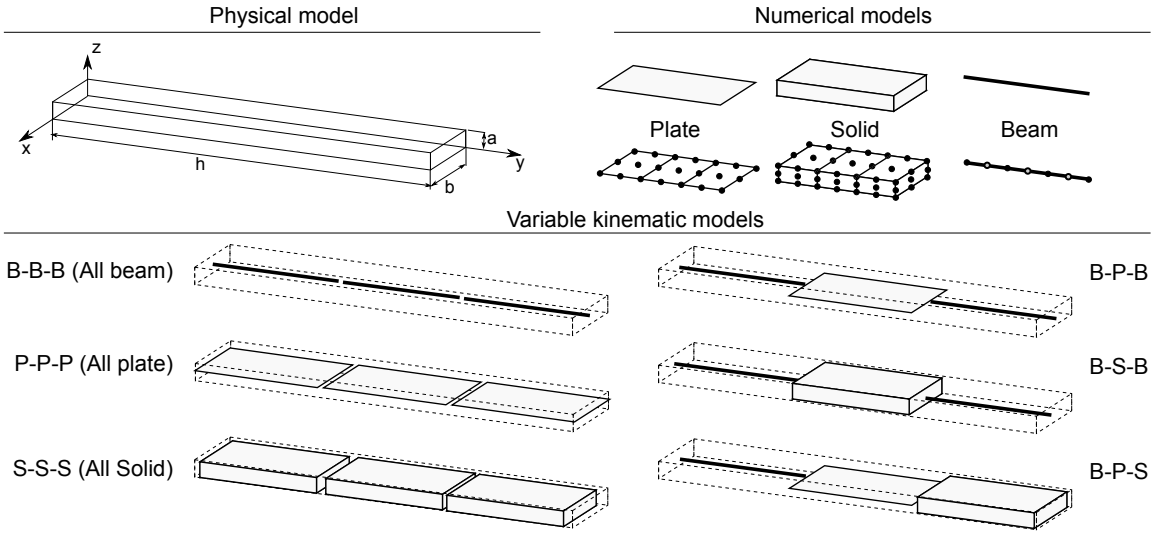

Fig. 8 Physical model of the cantilevered beam and different variable kinematics models of the structure (B=beam, P=plate and S=Solid)

models, beam, plate and shell, are considered. The structure is divided into three parts, each of

Table 1 Natural Frequencies of the cantilever beam Hz(B=beam, P=plate, S=solid)

Model	1^{st} bending mode X	1^{st} bending mode Z	1^{st} torsional mode
Euler-Bernoulli	58.7	117.4	394.9
B-B-B	58.6	116.0	426.5
P-P-P	58.4	115.7	429.4
S-S-S	58.8	116.2	426.2
B-S-B	58.7	116.1	426.2
B-B-S	58.7	116.2	426.1
S-B-B	58.7	116.1	426.2
B-P-B	58.5	115.9	428.2
B-P-S	58.6	115.9	427.9

these can be investigated with one of the introduced models. When the beam model is used, a 3-node element is used on the beam axis (quadratic) and a 9-node element on the cross-section. In the case of the plate elements, a 9-node element is used on the reference surface while a quadratic Lagrange expansion is considered over the thickness. When the solid model is considered, 27-node hexahedral elements are used.

The choice of the functions used in the models is arbitrary. To simplify the assembly procedure between different models in this work only quadratic functions have been used. In fact, when a 3-node beam element is combined with a 9-node element over the cross-section an advanced beam element with 27 nodes is obtained. Besides, when a 9-node plate element is combined with a quadratic Lagrange expansion through the thickness an advanced plate element with 27 nodes originates.

The model in which all the parts are considered as beams (B) is called B-B-B, but if the central part is considered as a solid (S), the model becomes B-S-B. The B-P-S model includes all the introduced structural models, including the plate (P) in the central part. Fig.8 shows some of these models from a graphical point of view, while several, obtained with the same approach, are considered in the analysis. Table 1 shows the results of the free vibration analysis of the cantilever beam. The considered models are reported in the first column. The second column shows the first bending frequency around the x axis while the first bending frequency around the z axis is reported in the third column. The last column shows the first torsional frequency. The first line shows the value of the bending frequencies obtained using the classical Euler-Bernoulli model. The results

show that all the used models are able to predict the dynamic behaviour of this structure with a very good accuracy. These results confirm that the introduced approach can be used to mix models with different kinematics without any loss of accuracy or the need to introduce new assumptions.

B. Reinforced panel analysis

The free vibration behaviour of a reinforced panel is investigated in this section. Figure 9 shows the geometry of the panel and the dimensions of the stringers. The square panel has edges of length $L = 1\ m$, while the thickness of the skin is $0.003\ m$. The panel is rounded by a 'I' reinforcement and has two stringers in the middle, one in the x direction and the other in the y direction. The dimensions of the cross-section of the reinforcements are $a = 0.03\ m$ and $b = 0.01\ m$. The considered material is isotropic (elastic modulus $E = 71.7\ GPa$, Poisson ratio $\nu = 0.3$ and density $\rho = 2700\ Kg/m^3$). The structure is not constrained. Figure 9 shows the characteristics of

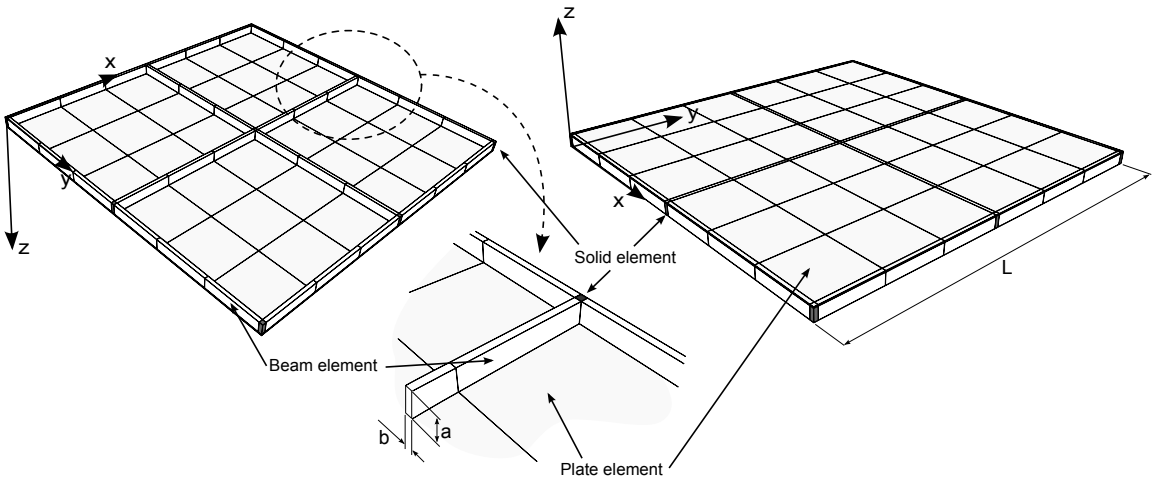

Fig. 9 Reinforced panel geometry

the variable kinematic model. The plate elements are used for the skin, three non uniform meshes are considered: a 9×9, a 11×11 and a 13×13. And a quadratic expansion is used through the thickness. Quadratic beam elements are used for the reinforcements, and a 9-node element is used over the cross-section. The number of beam elements is related to the skin mesh, more element are used over the skin, more elements are used along the beam axis. A 27-node solid element is used to connect the reinforcements to the skin at the cross-points. A full 3D model, solved using the $MSC\ Nastran$ commercial code, is used as a reference, eight-node elements were used. Table 2 shows the

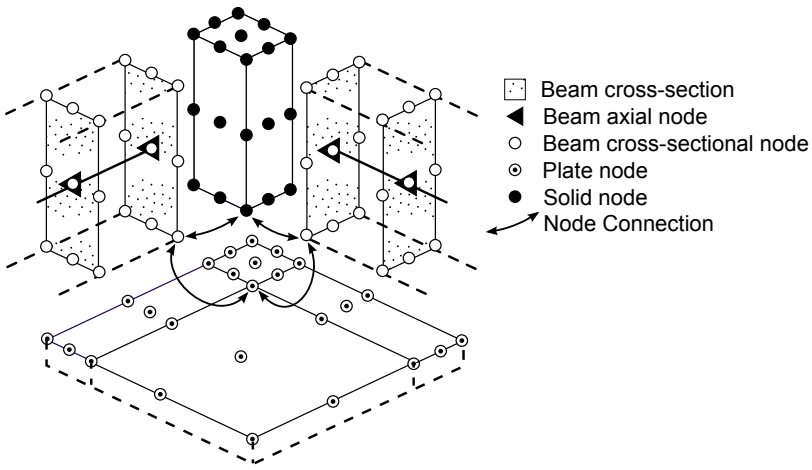

Fig. 10 Example of assembling of the mixed-dimensional model. In the corner the solid element connects the two beams and the plate.

	Present			Nastran
	9×9 Mesh	11×11 Mesh	13×13 Mesh	
Mode	4815 DOFs	6840 DOFs	8991 DOFs	21852 DOFs
1	20.6 $^{4.6\%}$	20.3 $^{3.0\%}$	20.2 $^{2.7\%}$	19.7
2	98.5 $^{1.4\%}$	98.1 $^{1.0\%}$	98.2 $^{1.1\%}$	97.1
3	$101.8^{1.0\%}$	$101.3^{0.5\%}$	101.5 $^{0.7\%}$	100.8
4	$109.4^{5.5\%}$	$107.7^{3.8\%}$	107.4 $^{3.6\%}$	103.7
5	$115.6^{5.1\%}$	$114.0^{3.7\%}$	113.8 $^{3.5\%}$	110.0
6	$115.6^{5.1\%}$	$114.1^{3.7\%}$	113.8 $^{3.5\%}$	110.0
7	$130.4^{2.0\%}$	$129.3^{1.2\%}$	129.5 $^{1.4\%}$	127.8
8	$130.4^{2.0\%}$	$129.5^{1.4\%}$	129.5 $^{1.4\%}$	127.8
9	$138.1^{5.3\%}$	$136.2^{3.8\%}$	136.0 $^{3.7\%}$	131.2
10	$212.8^{8.0\%}$	$204.5^{3.8\%}$	203.5 $^{3.3\%}$	197.0
11	$228.6^{9.4\%}$	$218.2^{4.5\%}$	216.8 $^{3.8\%}$	208.9
12	$228.6^{9.4\%}$	$218.5^{4.6\%}$	216.8 $^{3.8\%}$	208.9
13	$230.8^{9.7\%}$	$220.1^{4.6\%}$	218.4 $^{3.8\%}$	210.4
14	$251.8^{3.7\%}$	$248.4^{2.3\%}$	246.0 $^{1.3\%}$	242.9
15	$254.6^{9.7\%}$	$242.7^{4.6\%}$	240.7 $^{3.8\%}$	232.0
16	$254.6^{9.7\%}$	$242.6^{4.6\%}$	240.7 $^{3.8\%}$	232.0
17	$261.7^{10.8\%}$	$248.4^{5.2\%}$	248.3 $^{5.2\%}$	236.1

Table 2 First 17 Natural Frequencies of the reinforced panel [Hz]. Superscripts quote the percentage error with respect to the Nastran solution

first 17 natural frequencies of the reinforced panel. The second, third and fourth columns show the results obtained using the present model, while the fifth column shows the reference values. The natural frequencies evaluated using the present model are accurate. Only the modes that involve a larger number of half-waves show larger difference. These errors can be reduced using a refined mesh as in the case where a 13×13 mesh is used. Nevertheless, the present model allows the number of

DOFs to be reduced drastically.. Some of the modes are depicted in Figure 11. Figures 11a,b and c show some global modes. Figures 11d,e and f show more complex modes, where it is possible to see the effects of the reinforcements. Modes 10 and 12, see Figures 11e and f, have a higher number of half-waves and, as previously stated, refined mesh are required to reach good accuracy. The modal

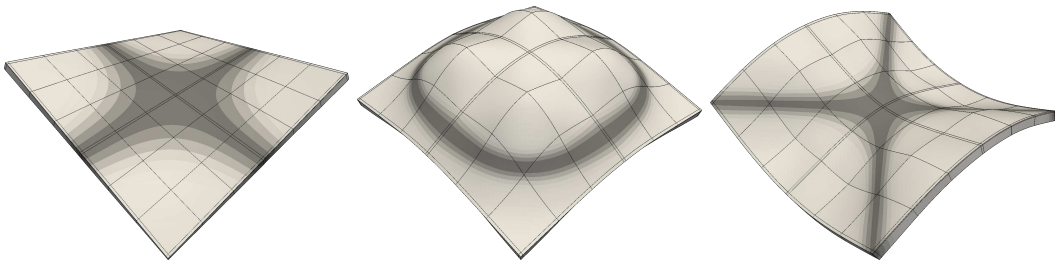

(a) Mode 1, 20.6 Hz (b) Mode 2, 98.5 Hz (c) Mode 3, 101.8 Hz

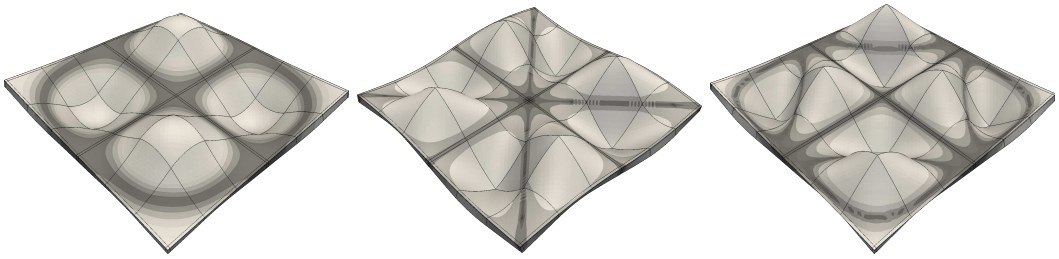

(d) Mode 4, 109.4 Hz (e) Mode 10, 212.8 Hz (f) Mode 13, 230.8 Hz

Fig. 11 Examples of the modal shapes of the reinforced panel evaluated using the present variable kinematic model with a 9×9 mesh.

shapes obtained using the present model have been compared with those from the reference model using the MAC criterion. Figure 12 shows the result of the MAC correlation. The modes evaluated with the present model are quite accurate, and only in some cases are there some differences. In particular, in the present model, there is a shift of the 14^{th} mode which appears as the 16^{th} in the reference model. The results of this analysis show that the present variable kinematic model provides accurate results for complex structures.

C. Simplified aircraft analysis

The free vibration response of a simplified aircraft model is considered in order to investigate the capabilities of the present model in the analysis of complex structures. The geometry of the structure is depicted in Figure 13. The dimensions are expressed as functions of parameter a, which is considered equal to 0.5 m. The structure has a constant thickness of $0.2 \times a$. No boundary conditions are applied, so the aircraft is completely free. As in pre previous case the material that

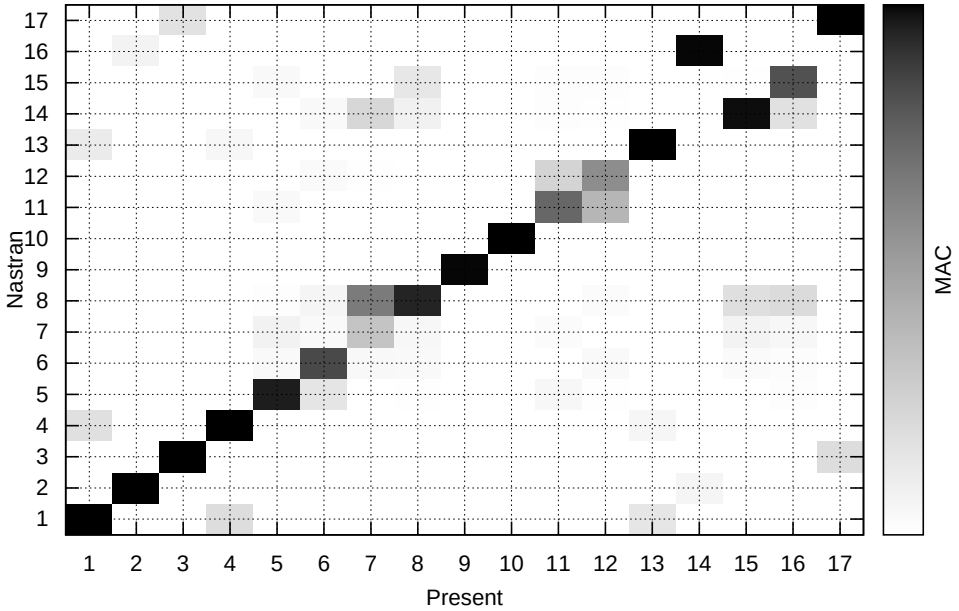

Fig. 12 MAC correlation between the present (9×9 Mesh) and the reference model. White=0, Black=1.

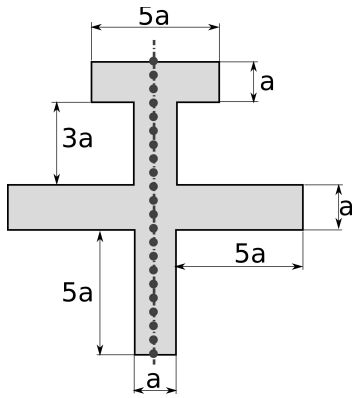

Fig. 13 Simplified aircraft model.

is used is aluminium. Different mixed-dimensional models are considered:

- 1D LE model with non-oriented beams (Fig14a)
- 1D LE model with oriented beams (Fig14b)
- 1D LE model with oriented beams + 2D elements (Fig14c)
- 1D LE model with oriented beams + 3D elements (Fig14d)

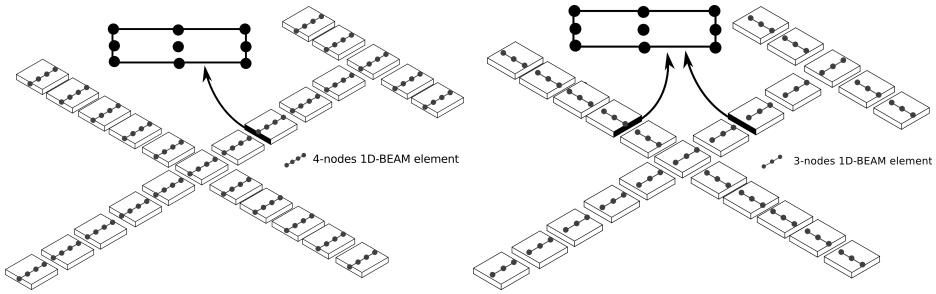

(a) 1D - Lagrange Expansion (LE) model (Mod1)

(b) 1D - Lagrange Expansion (LE) model (Mod2)

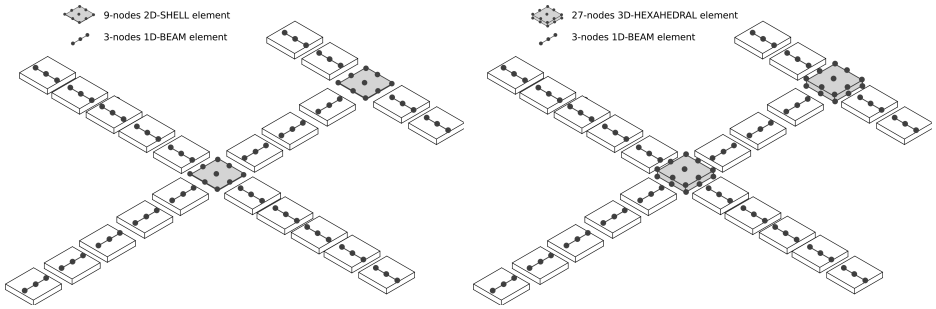

(c) 1D - Lagrange Expansion (LE) model + 2D shell elements

(d) 1D - Lagrange Expansion (LE) model + 3D hexahedral elements

Fig. 14 Models considered in the analysis.

	LE(Mod1)	LE(Mod2)	LE+2D	LE+3D	Nastran
DOFs	1845	1323	1323	1323	6120
1	10.94	10.93	10.92	10.93	10.80
2	18.20	18.17	18.18	18.18	17.26
3	20.21	20.20	20.20	20.21	20.05
4	50.40	50.55	50.62	50.80	50.37
5	52.12	51.61	51.62	51.62	51.16
6	52.39	52.98	52.98	52.98	51.31
7	66.96	67.48	67.48	67.48	65.55
8	70.63	71.78	71.78	71.77	69.94
9	77.84	76.60	76.69	76.69	75.77
10	89.57	88.55	88.59	88.59	87.44

Table 3 First ten natural frequencies of the simplified aircraft model.

When non-oriented beams are used, all the beam elements have the axis parallel to the fuselage axis as shown in Figure 14a. When oriented beams are used, the beam element used for the wings and the tails are rotated and the axis is now perpendicular to the fuselage axis, as shown in Figures 14b, c and d. The results, in terms of natural frequencies, are reported in Table 3. A 2D MSC Nastran model, built using four-nodes shell elements, is used as a reference. The degrees of freedom of each model are reported in the table. The results show that the analysis of a simplified aircraft

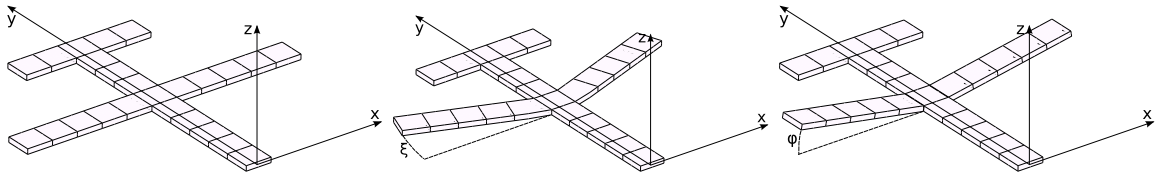

(a) Base model (b) Sweep angle (c) Dihedral angle

Fig. 15 Sweep angle and dihedral angles definition.

structure may be carried out by means of higher order one-dimensional models. The introduction of 2D elements and 3D elements, based on the CUF formulation, allows higher order 1D models, generally oriented in the space, do be connected, that is, complex structure can be analyzed with this approach

D. Sweep and dihedral angle effects

The same model presented in the previous section is here used. The approach presented in Figure 14b is adopted. Two new parameters are introduced, that is sweep and dihedral angles are considered in order to increase the complexity of the problem, as shown in Figure 15.

Three cases are considered: the base model, a model with a sweep angle (ξ) equal to 20 degrees and a model with a dihedral angle (φ) equal to 10. The results are compared with those from the two-dimensional model used in the previous section. Table 4 shows the first ten natural frequencies

	$\varphi = 0; \xi = 0$		$\varphi = 0; \xi = 20$		$\varphi = 10; \xi = 0$	
Mode	1D-LE	Nastran	1D-LE	Nastran	1D-LE	Nastran
1	$10.93^{1.1\%}$	10.80	$10.79^{3.0\%}$	10.47	$11.14^{1.6\%}$	10.96
2	$18.17^{5.2\%}$	17.26	$18.65^{4.9\%}$	17.77	$18.38^{4.1\%}$	17.66
3	$20.20^{0.7\%}$	20.05	$20.09^{4.7\%}$	19.19	$20.05^{1.6\%}$	19.73
4	$50.55^{0.4\%}$	50.37	$49.17^{-0.1\%}$	49.22	$44.72^{2.9\%}$	43.45
5	$51.61^{0.9\%}$	51.16	$51.41^{4.1\%}$	49.37	$52.35^{0.7\%}$	52.01
6	$52.98^{3.3\%}$	51.31	$56.39^{21.8\%}$	46.28	$59.51^{18.9\%}$	50.05
7	$67.48^{2.9\%}$	65.55	$70.16^{6.6\%}$	65.83	$66.97^{1.3\%}$	66.11
8	$71.78^{2.6\%}$	69.94	$72.21^{4.7\%}$	68.95	$74.29^{1.4\%}$	73.25
9	$76.60^{1.1\%}$	75.77	$78.32^{6.3\%}$	73.69	$78.91^{1.2\%}$	77.95
10	$88.55^{1.3\%}$	87.44	$89.14^{5.5\%}$	84.46	$89.04^{5.0\%}$	84.80

Table 4 First ten natural frequencies of the simplified aircraft model for different configuration. Superscripts quote the percentage error with respect the Nastran solution.

of the three different models. The results are compared with those from the commercial code, and the percentage difference between the present approach and the reference model is reported

in superscript. The reference model was built using four-node shell elements. The frequencies evaluated using the present approach appear to be very close to the reference; the differences in the frequency values are between 1% and 5%, and only the sixth mode shows a higher error than 10%. The first five modes for the three considered models are reported in Figure 17. MAC has been used in order to compare the results, in terms of modal shapes, with those from Nastran. The results are reported in Figure 16. The results of the base model show a very good correlation for the first ten modes. The model with a sweep angle equal to 20 degrees shows a good agreement, except for the sixth mode, which is the same that shows a discrepancy in the frequency. The model with a dihedral angle equal to 10 degrees shows a very good correlation, except for a switch between the fifth and the sixth modes. In conclusion the results show that the present model can be used with finite elements that have any orientation with respect to a given reference system

E. Analysis of an aircraft component

A typical aircraft structure is considered in this section. The structure is shown in Figure 18. It represents a part of a fuselage with the wing connection. Ribs, longerons and a thin skin are present in the same structure. The main dimensions of the structure are reported in Table 5. The entire

Dimensions $[m]$					
a=	3.000	d=	0.040	g	= 0.224
b=	3.160	e=	1.080	h	= 0.080
c=	6.000	f=	0.010	i	= 0.035

Table 5 Geometrical dimensions of the aircraft component.

structure is considered built with an aluminium alloy and with a Young modulus equal to 71.7 MPa, a Poisson ratio equal to 0.3 and a density of 2700 Kg/m^3. The structure is considered symmetric, so no displacements are allowed in the y direction for $y = 0$ and $y = b$. No displacement is allowed in the x direction for $x = 0$, while the displacement in z is free throughout. The whole structure is modelled using the one-dimensional model based on the Lagrange expansion. The fuselage is considered as a beam in the y direction with a variable cross-section in order to consider the ribs. The wing is also considered as a beam with the reference axis in the x direction. The structures are joined at the shared nodes. Two models derived using the present approach have been considered:

the first, Model 1, has a coarse mesh along the beam axis, while Model 2 has a more refined mesh and therefore a larger number of DOFs.

Mode	Model 1 (1D) 12153 DOFs	Model 2 (2D) 19797 DOFs	3D Nastran model (3D) 126782 DOFs
1	$0.00^{0.0\%}$	$0.00^{0.0\%}$	0.00
2	$3.92^{5.1\%}$	$4.09^{9.7\%}$	3.73
3	$22.54^{5.6\%}$	$22.66^{6.2\%}$	21.34
4	$23.94^{5.6\%}$	$24.02^{5.9\%}$	22.68
5	$25.22^{2.6\%}$	$25.56^{4.0\%}$	24.58
6	$27.98^{7.4\%}$	$27.68^{6.3\%}$	26.05
7	$37.32^{5.8\%}$	$37.57^{6.5\%}$	35.28
8	$41.52^{1.5\%}$	$42.15^{3.0\%}$	40.92
9	$51.12^{4.6\%}$	$50.30^{2.9\%}$	48.87
10	$67.56^{25.5\%}$	$66.93^{24.4\%}$	53.82

Table 6 First ten natural frequencies of the aircraft component considered.

The results, in terms of frequency, are reported in Table 6. The results are compared with those from the MSC Nastran commercial code evaluated by means of eight-node solid element model with more than 120000 DOFs. A MAC of Model 2 is compared with the Nastran model in Figure 19. Some modal shapes are shown in Figure 20. The results show that the present model can predict the complex dynamic behaviour of this structure well. The first ten frequencies show a good agreement with those from the commercial code, and only the tenth mode shows a higher difference in the frequency value than 10%. The first frequency is equal to 0, which means that a rigid body mode appears. The MAC analysis shows that the first 10 modes evaluated with the present models correspond with those evaluated with the reference model.

The modal shapes, see Figures 20a-i, show the first nine modes evaluated using Model 2. The model can predict both the global and local modes. In modes 2, 4 and 6, both fuselage and wing show a significant deformation, while modes 5, 8 and 10 involve only a part of the structure, the wing or the fuselage. Other modes, such as mode 9, include only a small part of the structure, in this case, the deck.

The results show that the present model can predict very complex deformations that can usually not be predicted by means of classical beam models.

F. Conclusions

An advanced variable kinematic model has been introduced in the present paper. A unified formulation that is able to derive one-, two- and three-dimensional models and which is based on Carrera Unified Formulation, has been considered. A family of refined structural elements has been introduced and the kinematic assumptions have allowed only displacements to be considered as the unknowns. These models were used to derive a variable kinematic model that is able to use one-, two- and three-dimensional models at the same time. The dynamics of a simple cantilever beam was investigated to assess the model. The variable kinematic model was the used to investigate more complex structures, that is, a reinforced panel and a simplified aircraft. Finally, a complex aircraft structure was investigated. The obtained results have been compared with those from the MSC Nastran commercial code. The MAC criterion was used to compare the modal shapes. From the results it is possible to state that:

- The refined structural models used in the present paper are able to overcome the limitations of classical models.
- The present approach allows 1D, 2D and 3D elements to be joined *naturally*, that is, no *ad hoc* techniques are required to join plates to beams, plates to solids or beams to solids.
- The obtained results show good accuracy compared to those obtained with commercial codes. Moreover, the computational cost can be reduced drastically.
- Complex geometries and structural configurations can be investigated.

Future works could be directed towards assessing the proposed variable kinematic model for stress analysis, buckling and dynamic response. It could also be extended to aircraft structures made of composite materials.

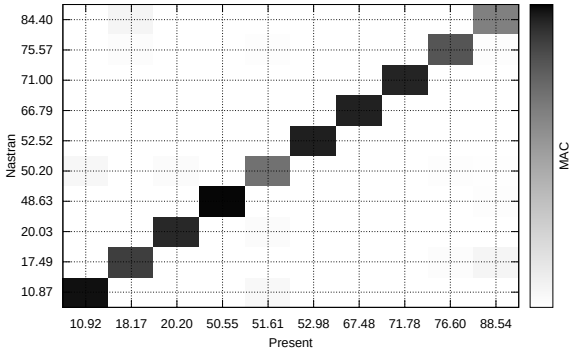

(a) $\varphi = 0; \xi = 0$

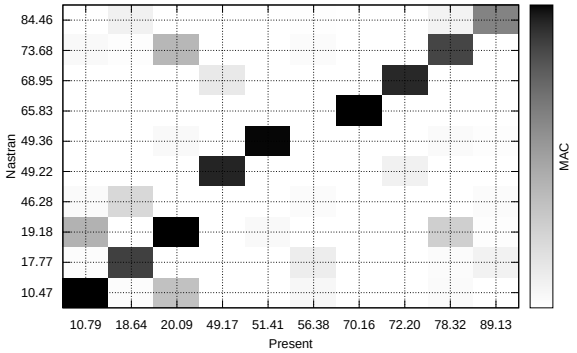

(b) $\varphi = 0; \xi = 20$

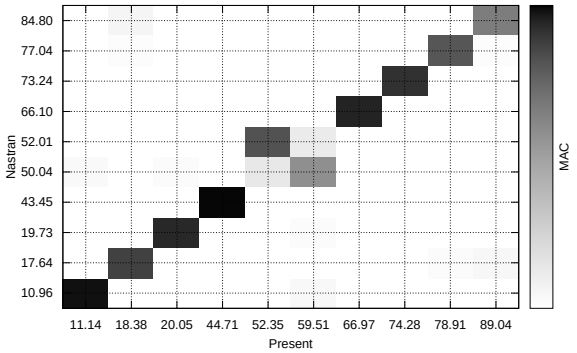

(c) $\varphi = 10; \xi = 0$

Fig. 16 Results of the MAC. analysis. On x axis are shown the first ten frequencies of the present model, on y axis the reference frequency.

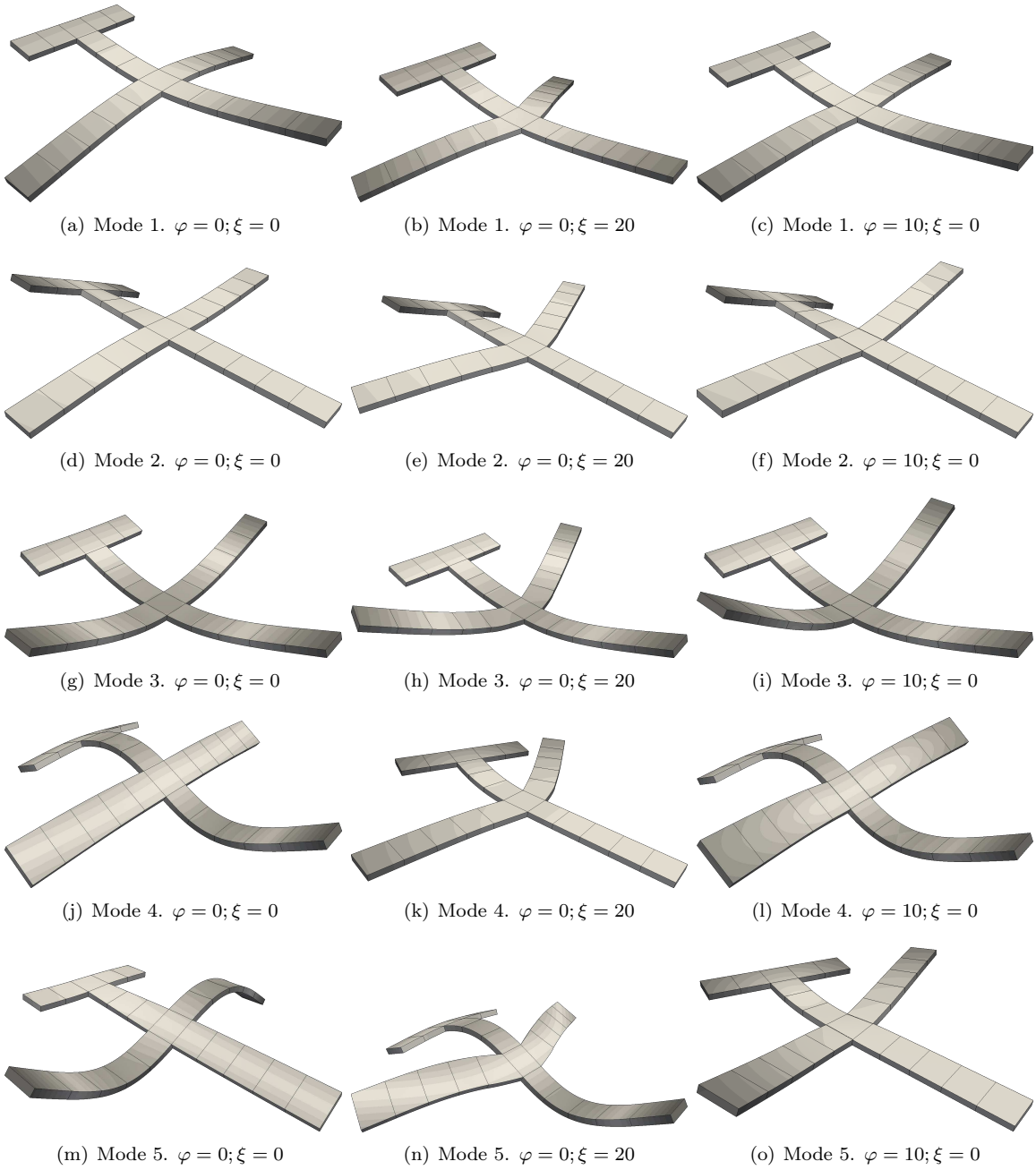

(a) Mode 1. $\varphi = 0; \xi = 0$ (b) Mode 1. $\varphi = 0; \xi = 20$ (c) Mode 1. $\varphi = 10; \xi = 0$

(d) Mode 2. $\varphi = 0; \xi = 0$ (e) Mode 2. $\varphi = 0; \xi = 20$ (f) Mode 2. $\varphi = 10; \xi = 0$

(g) Mode 3. $\varphi = 0; \xi = 0$ (h) Mode 3. $\varphi = 0; \xi = 20$ (i) Mode 3. $\varphi = 10; \xi = 0$

(j) Mode 4. $\varphi = 0; \xi = 0$ (k) Mode 4. $\varphi = 0; \xi = 20$ (l) Mode 4. $\varphi = 10; \xi = 0$

(m) Mode 5. $\varphi = 0; \xi = 0$ (n) Mode 5. $\varphi = 0; \xi = 20$ (o) Mode 5. $\varphi = 10; \xi = 0$

Fig. 17 First five modal shapes for the different models considered.

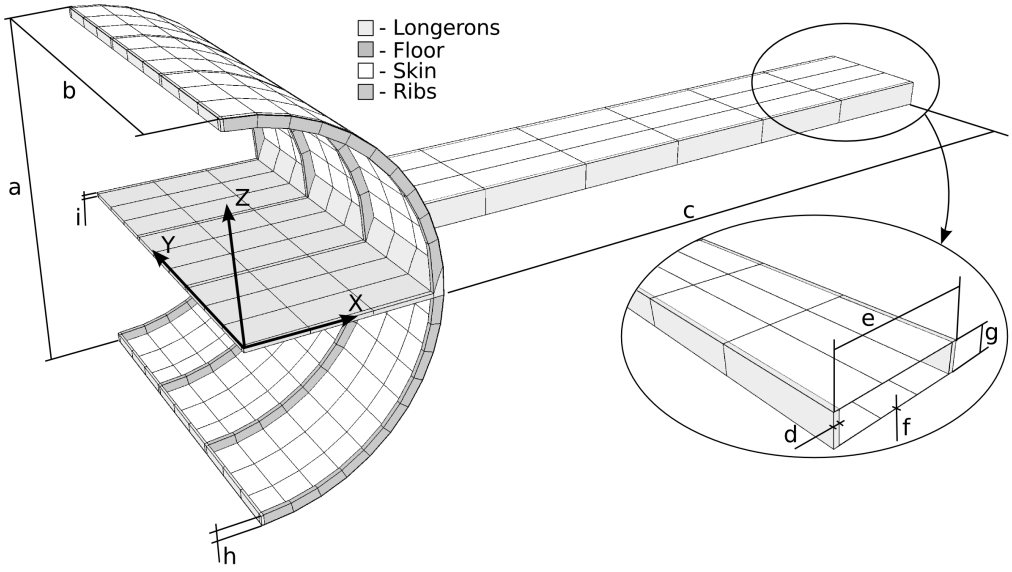

Fig. 18 Aircraft structure considered.

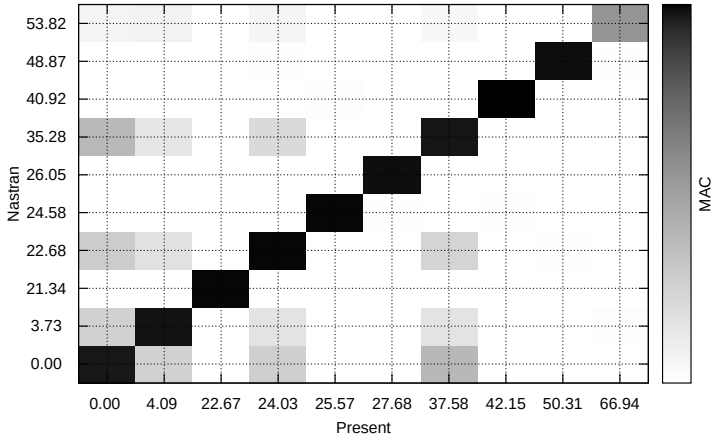

Fig. 19 MAC analysis, comparison between the present Model 2 with respect to the 3D Nastran Model.

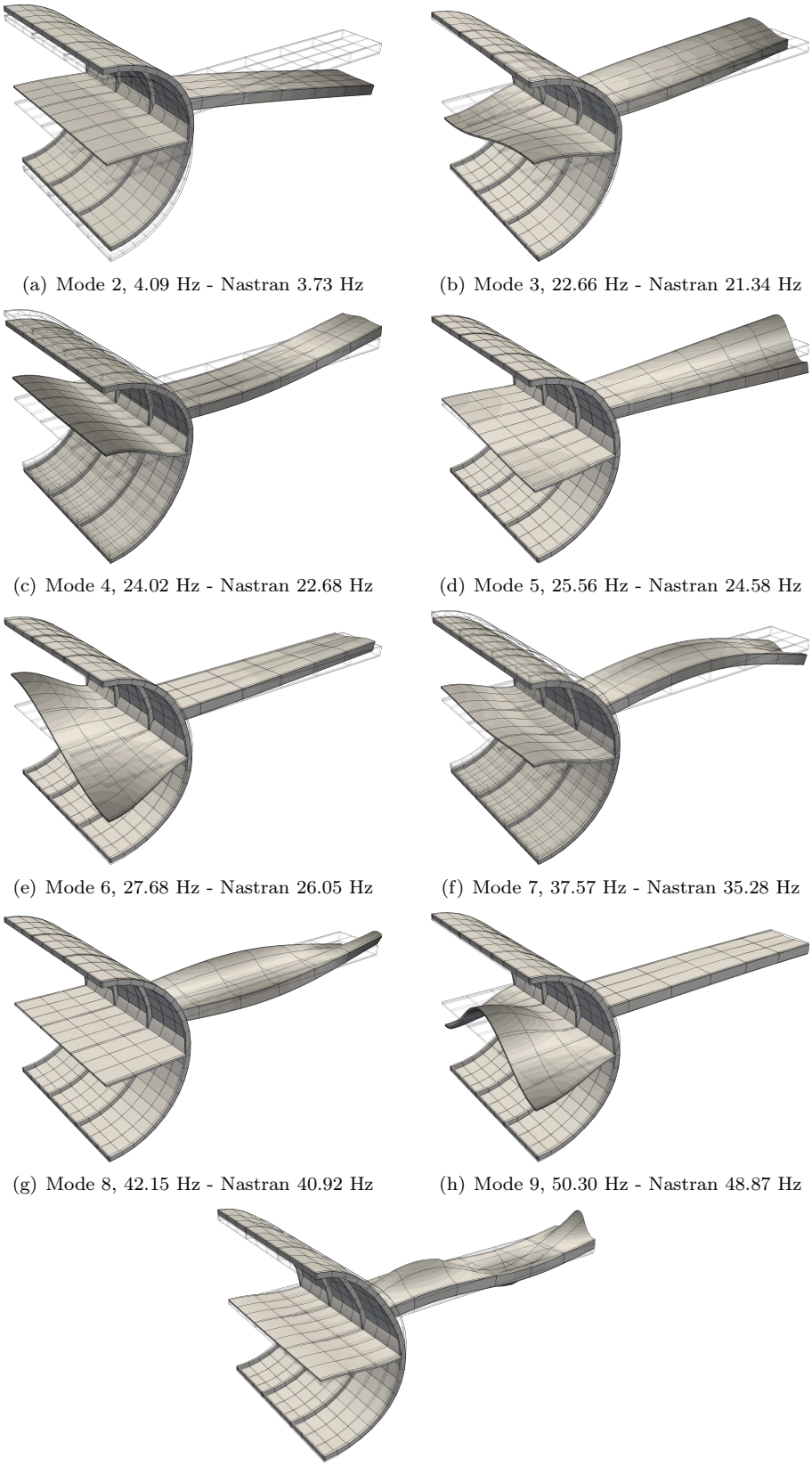

(a) Mode 2, 4.09 Hz - Nastran 3.73 Hz

(b) Mode 3, 22.66 Hz - Nastran 21.34 Hz

(c) Mode 4, 24.02 Hz - Nastran 22.68 Hz

(d) Mode 5, 25.56 Hz - Nastran 24.58 Hz

(e) Mode 6, 27.68 Hz - Nastran 26.05 Hz

(f) Mode 7, 37.57 Hz - Nastran 35.28 Hz

(g) Mode 8, 42.15 Hz - Nastran 40.92 Hz

(h) Mode 9, 50.30 Hz - Nastran 48.87 Hz

(i) Mode 10, 66.93 Hz - Nastran 53.82 Hz

Fig. 20 First 9 modal shapes of the aircraft component considered.

References

[1] Argiris, J. M. and Kelsey, S., *Energy theorems and structural analysis*, Butterworths, 1960.

[2] Bruhn, E. F., *Analysis and design of flight vehicle structures*, Tri-State Offset Company, 1973.

[3] Carrera, E., *Fondamenti sul calcolo si strutture a guscio rinforzato per veicoli aerospaziali*, Levrotto e Bella, Torino, 2011.

[4] Zienkiewicz, O. and Taylor, R., *The Finite Element Method for Solid and Structural Mechanics*, Elsevier Butterworth-Heinemann, Oxford, sixth edition ed., 2000.

[5] Euler, L., *De curvis elasticis*, Lausanne and Geneva: Bousquet, 1744.

[6] Timoshenko, S. P., "On the corrections for shear of the differential equation for transverse vibrations of prismatic bars," *Philosophical Magazine*, Vol. 41, 1921, pp. 744–746.

[7] Love, A. E. H., "The Small Free Vibrations and Deformation of a Thin Elastic Shell," *Philosophical Transactions of the Royal Society of London A: Mathematical, Physical and Engineering Sciences*, Vol. 179, 1888, pp. 491–546.

[8] Reissner, E., "The effect of transverse shear deformation on the bending of elastic plates," *ASME Journal of Applied Mechanics*, Vol. 12, 1945, pp. 68–77.

[9] Mindlin, R. D., "Influence of rotatory inertia and shear on flexural motions of isotropic elastic plates," *ASME Journal of Applied Mechanics*, Vol. 18, 1951, pp. 31–38.

[10] Argiris, "Matrix analysis of three-dimensional elastic media small and large displacements." *AIAA Journal*, Vol. 3, No. 1, 1965, pp. 45–51.

[11] Strang, *Calculus*, Welles-Cambridge Press, 1991.

[12] Ben Dhia, H., "Multiscale mechanical problems: the arlequin method," *Comptes Rendus de l'Academie des Sciences Series IIB Mechanics Physics Astronomy*, Vol. 326, No. 12, 1998, pp. 899–904.

[13] Ben Dhia, H. and Rateau, H., "The arlequin method as a flexible engineering tool," *International journal for numerical methods in engineering*, Vol. 62, No. 11, 2005, pp. 1442–1462.

[14] McCune, R., Armstrong, C., and Robinson, D., "Mixed-dimensional coupling in finite element models," *International Journal for Numerical Methods in Engineering*, Vol. 49, 2000, pp. 725–750.

[15] Garusi, E. and Tralli, A., "A hybrid stress-assumed transition element for solid-to-beam and plate-to-beam- connections," *Computers and structures*, Vol. 80, 2002, pp. 105–115.

[16] Song, H. and Hodges, D., "Rigorous Joining of Asymptotic Beam Models to Three-Dimensional Finite Element Models," *Computer Modeling in Engineering and Sciences*, Vol. 85, No. 5, 2012, pp. 239–278.

[17] Blanco, P., Feijóo, R., and S.A., U., "A variational approach for coupling kinematically incompatible structural models," *Computer Methods in Applied Mechanics and Engineering*, Vol. 197, No. 17-18,

2008, pp. 1577–1602.

[18] Davila, C., "Solid-to-shell transition elements for the computation of interlaminar stresses," *Computing Systems in Engineering*, Vol. 5, 1994, pp. 193–202.

[19] Shim, K., Monaghan, D, J., and Armstrong, C., "Mixed dimensional coupling in finite element stress analysis," *Engineering with Computers*, Vol. 18, 2002, pp. 241âĂŞ252.

[20] Luan, Y., Ohlrich, M., and Jacobsen, F., "Improvements of the smearing technique for cross-stiffened thin rectangular plates," *Journal of Sound and Vibration*, Vol. 330, 2011, pp. 4274–4286.

[21] Edalat, P., Khedmati, M., and Guedes Soares, C., "Free Vibration and Dynamic Response Analysis of Stiffened Parabolic Shells using Equivalent Orthotropic Shell Parameters." *Latin American Journal of Solids and Structures*, Vol. 10, 2013, pp. 747–766.

[22] Mustafa, B. and Ali, R., "Prediction of natural frequency of vibration of stiffened cylindrical shells and orthogonally stiffened curved panels," *Journal of Sound and Vibration*, Vol. 113, 1987, pp. 317–327.

[23] Edward, A. and Samer, A., "A fnite element model for the analysis of stiffened laminated plates," *Computers and Structures*, Vol. 20, 2000, pp. 369–383.

[24] Yu, W., Volovoi, V. V., Hodges, D. H., and Hong, X., "Validation of the variational asymptotic beam sectional analysis (VABS)," *AIAA Journal*, Vol. 40, 2002, pp. 2105–2113.

[25] Yu, W., Hodges, D., and Jimmy, C., "Variational Asymptotic Beam Sectional Analysis – An Updated Version," *International Journal of Engineering Science*, Vol. 59, 2012, pp. 40–64.

[26] Carrera, E., "A class of two dimensional theories for multilayered plates analysis," *Atti Accademia delle Scienze di Torino, Memorie Scienze Fisiche*, Vol. 19-20, 1995, pp. 49–87.

[27] Carrera, E., "Multilayered Shell Theories that Account for a Layer-Wise Mixed Description. Part I. Governing Equations," *AIAA Journal*, Vol. 37, 1999, pp. 1107–1116.

[28] Carrera, E., "Multilayered Shell Theories that Account for a Layer-Wise Mixed Description. Part II. Numerical Evaluations." *AIAA Journal*, Vol. 37, 1999, pp. 1117–1124.

[29] Carrera, E., "A Reissner's Mixed Variational Theorem Applied to Vibration Analysis of Multilayered Shell," *Journal of Applied Mechanics*, Vol. 66, 1999, pp. 69–78.

[30] Carrera, E. and Zappino, E., "Full Aircraft Dynamic Response by Simplified Structural Models," *Proceedings 54rd AIAA/ASME/ASCE/AHS/ASC Structures, Structural Dynamics, and Materials Conference (SDM)*, Boston, Massachusetts, USA, April 8-11 2013.

[31] Carrera, E., Giunta, G., and Petrolo, M., *Beam Structures: Classical and Advanced Theories.*, John Wiley & Sons Ltd., 2011, ISBN 9780470972007.

[32] Carrera, E. Brischetto, S. and Nali, P., *Plates and Shells for Smart Structures: Classical and Advanced*

Theories for Modeling and Analysis, John Wiley & Sons, 2011.

[33] Carrera, E., Cinefra, M. Petrolo, M., and Zappino, E., *Finite Element Analysis of Structures Through Unified Formulation*, John Wiley & Sons, 2014, In press.

[34] Carrera, E., Petrolo, M., and Zappino, E., "Performance of CUF approach to analyze the structural behavior of slender bodies," *Journal os Structural Engineering*, 2011, Available on-line, DOI: 10.1061/(ASCE)ST.1943-541X.0000402.

[35] Carrera, E., Zappino, E., and Petrolo, M., "Analysis of thin-walled structures with longitudinal and transversal stiffeners," *Journal of Applied Mechanics*, Vol. 80, No. 1, 2013, pp. 011006–1–011006–12.

[36] Cinefra, M., Chinosi, C., and Della Croce, L., "MITC9 shell elements based on refined theories for the analysis of isotropic cylindrical structures." *Mechanics of Advanced Materials ans Structures*, Vol. 20, 2013, pp. 91–100.

[37] Carrera, E., Pagani, A., and Petrolo, M., "Use of Lagrange multipliers to combine 1D variable kinematic finite elements." *Computers & Structures*, Vol. 129, 2013, pp. 194–206.

[38] Biscani, F., Giunta, G., Belouettar, S., Carrera, E., and Hu, H., "Variable kinematic beam elements coupled via Arlequin method," *Composite Structures*, Vol. 93, 2011, pp. 697–708.

[39] Oñate, E., *Structural Analysis with the Finite Element Method: Linear Statics, Volume 1*, Springer, Barcelona, Spain, 2009.

[40] Carrera, E., Giunta, G., Nali, P., and Petrolo, M., "Refined beam elements with arbitrary cross-section geometries," *Computers and Structures*, Vol. 88, No. 5–6, 2010, pp. 283–293, DOI: 10.1016/j.compstruc.2009.11.002.

[41] Carrera, E. and Petrolo, M., "Refined Beam Elements with only Displacement Variables and Plate/Shell Capabilities," *Meccanica*, Vol. 47, 2012, pp. 537–556.

APPENDIX A: EXPLICIT FORMULATION OF THE LAGRANGE POLYNOMIALS

The present work uses the Lagrange polynomials to describe the displacement field of beam, shell and solid elements. The Lagrange polynomials are widely used in classical FE models and the description of these functions can be found in many books, one example is the book by Oñate [39]. The Lagrange functions are expressed in the natural reference system therefore they range between ± 1. The iso-parametric formulation is used to switch between the natural and the physical reference system. The Lagrange functions allow the displacement field to be completely derived from the displacement in a finite number of points, called nodes. Different number of nodes can be

used to increase the order of the functions. In the present work only quadratic functions will be introduced.

One-dimensional Lagrange functions are used to describe the displacement along the beam axis and through the plate thickness, they have the following formulation.

External nodes:

$$F_\tau = \frac{1}{2}(r^2 - r) \qquad \tau = 1 \tag{A1}$$

$$F_\tau = \frac{1}{2}(r^2 + r) \qquad \tau = 3 \tag{A2}$$

Central node:

$$F_\tau = (1 - r^2) \qquad \tau = 2 \tag{A3}$$

Where r is the coordinate of the 1D natural reference system while r_τ is the value of the coordinate in the $\tau - th$ node.

Two-dimensional Lagrange functions are used to describe the displacement over the beam cross-section and over the plate reference surface, they have the following formulation.

Corner nodes:

$$F_\tau = \frac{1}{4}(r^2 + r\ r_\tau)(s^2 + s\ s_\tau) \qquad \tau = 1, 3, 5, 7 \tag{A4}$$

Mid-side nodes:

$$F_\tau = \frac{1}{2}s_\tau^2(s^2 - s\ s_\tau)(1 - r^2) + \frac{1}{2}r_\tau^2(r^2 - r\ r_\tau)(1 - s^2) \qquad \tau = 2, 4, 6, 8 \tag{A5}$$

Central node:

$$F_\tau = (1 - r^2)(1 - s^2) \qquad \tau = 9 \tag{A6}$$

Where s and r are the coordinates of the 2D natural reference system, while s_τ and r_τ are the values of the coordinates in the $\tau - th$ node.

Three-dimensional Lagrange functions are used to describe the displacement when solid elements

are considered, they have the following formulation.

Corner nodes:

$$F_\tau = \frac{1}{8}(r^2 + r\ r_\tau)(s^2 + s\ s_\tau)(t^2 + t\ t_\tau) \qquad \tau = 1, 3, 5, 7, 19, 21, 23, 25 \tag{A7}$$

Mid-side nodes:

$$F_\tau = \frac{1}{4}s_\tau^2(s^2 - s\ s_\tau)r_\tau^2(r^2 - r\ r_\tau)(1 - t^2) + \frac{1}{4}s_\tau^2(s^2 - s\ s_\tau)t_\tau^2(t^2 - t\ t_\tau)(1 - r^2) +$$
$$\frac{1}{4}r_\tau^2(r^2 - r\ r_\tau)t_\tau^2(t^2 - t\ t_\tau)(1 - s^2) \qquad \tau = 2, 4, 6, 8, 10, 12, 14, 16, 20, 22, 24, 26 \tag{A8}$$

Face central nodes:

$$F_\tau = \frac{1}{2}(1 - r^2)(1 - s^2)(t + t_\tau t^2) + \frac{1}{2}(1 - r^2)(1 - t^2)(s + s_\tau s^2) +$$
$$\frac{1}{2}(1 - t^2)(1 - s^2)(r + r_\tau r^2) \qquad \tau = 9, 11, 13, 15, 17, 27 \tag{A9}$$

Internal central node:

$$F_\tau = (1 - r^2)(1 - s^2)(1 + t^2) \qquad \tau = 18 \tag{A10}$$

Where s, r and t are the coordinates of the 3D natural reference system, while s_τ, r_τ and t_τ are the values of the coordinates in the $\tau - th$ node.